Optical Strain Measurement of an Inflated Cylinder using Photogrammetry with Application to Scientific Balloons

Joseph R. Blandino[*]
James Madison University, Harrisonburg, VA 22807

Jerry Sterling.[†]
NASA Wallops Flight Facility, Wallops Island, VA 23337

Frank Baginski[‡] and Eric Steadman[§]
George Washington University, Washington, D.C. 20052

Jonathan T. Black[**]
University of Kentucky, Lexington, KY 40506

And
Richard S. Pappa[††]
NASA Langley Research Center, Hampton, VA 23681

A study is presented using photogrammetry to measure the biaxial strain in an inflated cylinder. Two cylinders constructed from polyethylene and each approximately 222 mm in diameter and 930 mm in length were studied. The first had a 0.038 mm wall thickness while the second had a 0.02 mm wall thickness. The cylinders were inflated to a maximum pressure of 1379 Pa. The strain was determined from data collected from 60 retro-reflective targets arranged in a 12 x 5 grid. The uncertainty of the measurement system was determined to be 0.08, 0.04 and 0.06 mm in the x, y, and z directions respectively. The hoop and meridional strains determined from displacement data were compared to values obtained from a finite element analysis of a related proxy problem. The predicted hoop strains showed good agreement over the entire range of pressures while the meridional strains showed good agreement at the lower pressures.

Nomenclature

E	=	Modulus of Elasticity
E_T	=	Total Energy
E_p	=	Potential Energy
L	=	Length of cylinder
P	=	Pressure
r	=	Cylinder Radius
S	=	Membrane surface configuration
t	=	Cylinder wall thickness
W^*_f	=	Relaxed film strain energy
ε_θ	=	Hoop Strain
ε_ϕ	=	Meridonal Strain

[*] Associate Professor, Integrated Science and Technology, MSC 4310, AIAA Senior Member.
[†] Materials Engineer, Balloon R&D Laboratory, AIAA Member.
[‡] Professor, Department of Mathematics. AIAA Senior Member.
[§] Graduate Research Assistant, Department of Mathematics.
[**] Graduate Research Assistant, Department of Mechanical Engineering, AIAA Student Member.
[††] Senior Research Engineer, Structural Dynamics Branch, AIAA Senior Member.

ε_1 = First Principal Strain
ε_2 = Second Principal Strain
σ_θ = Hoop stress
σ_ϕ = Meridonal Stress
σ_1 = First Principal stress
σ_2 = Second Principal Stress
N_1 = First Principal Stress Resultant
N_2 = Second Principal Stress Resultant
ν = Poisson's ratio
θ = Angular position on cylinder

I. Introduction

The optimum design and operation of any structure requires appropriate knowledge of the properties of its material components. For the NASA scientific balloons program, the mechanical properties of the thin film material composing the gaseous envelope have primarily been studied uniaxially over the two primary axes, such as with traditional tensile analysis in the film machined and transverse directions. However, for thorough understanding of structural behavior, a minimally intrusive study of candidate materials in a loading environment more similar to flight conditions provides more useful information. The material behavior in a multi-axial loading situation is somewhat illuminated by the traditional measurement of Poisson's ratios, wherein the change in dimension of a specimen in a direction perpendicular to an applied load is compared to the change in dimension along the loading axis. However, balloons are loaded biaxially, and all three dimensions of the envelope film may change in response to this load. With the recent application of photogrammetry to study the static and dynamic behavior of Gossamer space structures such as solar shields and inflatable booms, the NASA Balloons Program Office sees an opportunity to study balloon model structures, and potentially even full scale balloons in flight, for their dynamic response to applied load in the form of internal pressurization. By characterizing a number of representative model structures, and then comparing the change in response of these models when constructed of different materials, we intend to demonstrate the capacity to investigate materials in three dimensional loading environments.

This paper presents a combined experimental and numerical study investigating the stress in an inflated cylinder. Stress and strain values are obtained using photogrammetry. A finite element analysis of an inflated cylinder is carried out and the numerical results are compared to the experimental data.

II. Balloon Biaxial Strain Measurement History

The principle challenge in measuring strain and other dynamic quantities in scientific balloons, their related model structures, and other structures employing thin polymer films to bear load, is to make accurate measurements without the instrument significantly affecting the local or global state of the structure or material. While non-contact methods such as photogrammetry would be the ideal means, other approaches have been used to advance the art and science of gossamer craft over the decades. The literature of scientific ballooning technology was surveyed to provide context to our current work, and our goals with this work are in close alignment with those of the works discussed below, reflecting a continuing need to develop the technology.

In 1965, Stautgaitis and Kobren[1] of NASA-Goddard reported a collaborative effort with the U.S. Army Map Service to measure the skin strain of a full-scale Echo II passive communications reflector balloon during inflation tests in a hangar. Their first tests (June 1963) used a painted-on grid pattern and suffered from "grid line width variability" and "inadequate pattern size." Changing to a precision dot pattern improved the data quality, but indicated the need for improved lighting conditions due to both washed-out and dark sections. Two RC-8 Wild aerial cameras modified to a fixed focal distance (12.9 ft.) were the photographic instruments. They reported reasonable correlation between measurements and calculated predictions given the limitations of the experimental technique and the assumptions pertaining to material properties used in the analysis.

Following the Echo II work and through about 1995, the measurement of strain in balloons and related model structures shifted away from photogrammetric methods, although significant progress was made in biaxial stress-strain experimental techniques. In experiments using pressurized polyethylene cylinders to study material properties, Alexander[2] determined strain by measuring the changing location of benchmarks using vernier calipers. At about the same time, Kawada and coworkers were developing a soft strain gauge[3] to overcome incompatibilities between common strain gauges and balloon films. The soft gauges comprised a thin Nickel-Copper wire mounted on

a polyethylene film base, and were used on small model balloons in the laboratory at room and reduced temperatures, and in flight on a 6-meter polyethylene balloon. The Kawada group then developed a strain slide gauge[4] based on a resistor coil for use on balloon flights. Although these gauges were relatively heavy (tens of grams), their response was stable over the wide range of temperatures experienced by scientific balloons in flight.

In the early 1980's, Rand[5] developed a strain gauge comprising four foil strain gauges bonded to a flexible ring and connected in a Wheatstone bridge circuit. They were demonstrated in the laboratory to measure model balloon strains, to collect uniaxial creep data, and to measure the coefficient of thermal expansion, and were then flown successfully on a 28,320 m^3 balloon.[6] Rand gauges were also used by Simpson to study model balloons in a hangar,[7] leading to the first comparison of in-flight (500 m^3 balloon) strain measurements to structure predictions from finite element analysis.[8] Martone applied these gauges to the study of material properties using inflated cylinders in the laboratory,[9] and, because the small curvature radius of the lab-scale cylinders introduced a non-negligible strain measurement offset, determined the correction factor using flexible scales. The flexible scales were described by Said[10,11] as transparency sheets with a printed one-millimeter scale, with strain indicated by scale movement versus a drawn or affixed benchmark.

In the mid-1990's, Rand and Grant (Fairbrother) developed an optical technique for measuring biaxial film strains using an applied random speckle pattern and a CCD camera with digital image correlation software[12]. The speckle pattern was applied to a small section of an inflated cylinder. The area covered approximately 150 x 150 pixels. The technique was used with pressurized cylinder experiments to develop a nonlinear viscoelastic constitutive representation for the material.[13]

Photogrammetry is an optical measurement technique that has been used to characterize the static shape of Gossamer structures.[14-18] By triangulating from known camera positions to the location of identical targets on a series of photographs, a three dimensional model of an imaged surface can be obtained. The imaged targets are usually circular and are either projected or physically attached to the surface of the structure. Projected targets have the advantage of not altering the surface of the structure, but the structure can move independently of the projected targets. Fixed targets add mass and local stiffness to the structure, but they move with the structure so changes in the relative position of the targets can be used to determine the strain. The disadvantages of additional mass and stiffness can be minimized by the proper selection of targets.

III. Experimental Study

Analytical Development

An inflated cylinder is analyzed as a thin walled pressure vessel. If the radius, pressure and wall thickness is known the hoop and meridional stress is determined from:

$$\sigma_H = \frac{\mathrm{Pr}}{t} \tag{1}$$

$$\sigma_M = \frac{\mathrm{Pr}}{2t} \tag{2}$$

If the ends of the cylinder are constrained the corresponding strains are defined as:

$$\varepsilon_H = \frac{\Delta r}{r} = \frac{1}{E}(\sigma_H - \nu\sigma_M) \tag{3}$$

$$\varepsilon_M = \frac{\Delta L}{L} = \frac{1}{E}(\sigma_M - \nu\sigma_H) \tag{4}$$

Substituting Eqns (1) and (2) into Eqns (3) and (4) gives expressions for the strains in terms of the applied pressure, cylinder radius and material thickness.

$$\varepsilon_H = \frac{\mathrm{Pr}}{2Et}(2 - \nu) \tag{5}$$

$$\varepsilon_M = \frac{\mathrm{Pr}}{2Et}(1 - 2\nu) \tag{6}$$

The use of a linear, isotropic material constitutive relation is at least a reasonable starting point for our work at low stresses, small deformations, short durations, and steady temperature. Because properties of the polyethylene film were unknown to us for the conditions under which the photogrammetry data was collected, we used estimates for the Poisson ratio and Youngs modulus and assumed the thicknesseses were known. To determine strain, the measurement system must monitor pressure and cylinder radius. From Eqn (4) the meridional strains may also be obtained from a change in spacing of measured points along the cylinder length.

Test set-up

The test articles (2) for this study were polyethylene cylinders. Material was heat seamed to form a cylinder approximately 222.0 mm in diameter. Seaming was done by hand and there was some variation in diameter along the length of the cylinder. The polyethylene used to fabricate the first cylinder was 0.038 mm (1.5 mil), while 0.02 mm (0.8 mil) thick material was used for the second. Sixty retro-reflective targets were fixed in a 12 x 5 grid pattern near the center of the cylinder. The targets were approximately 3 mm in diameter and target spacing was approximately 25 mm x 38 mm.

The cylinder was attached to an aluminum test frame shown in Fig. 1. Aluminum end-caps were supported by a 6.35 mm thick x 50 mm wide aluminum bar. The end-caps were spaced 930.3 mm (36.625 in) apart. Each end-cap had a port with barb fitting that was used either for inflation or the attachment of a pressure transducer. The end-caps had a thin gasket around the edge where it contacted the polyethylene cylinder. The balloon was fastened to the end-caps using hose clamps. The cylinders were inflated using compressed air, and the inflation rate was controlled manually using a pressure-regulating valve. The cylinders were inflated to a maximum pressure of 1379 Pa (0.2 psi) above atmospheric pressure.

As the cylinder was inflated the shape was recorded using a four-camera photogrammetry system. The cameras used had 5.0 megapixel (2560 x 1920) resolution. The cylinder was inflated slowly and maintained at a desired pressure while images were captured. The inflation rate was slow and the change in pressure between measurements small therefore, it was assumed that the cylinder did not undergo viscoelasic relaxation. The cameras were set for a 1/640 second exposure. The camera flash intensity was muted using several layers of masking tape. This provided images with excellent contrast. A typical image set is shown in Fig. 2. Image sets were processed using commercially available photogrammetry software. Image scale and axes were set using scale tape. The tape can be seen in Fig. 1 running the length of the test rig and also vertically below the balloon. The tape had 3 mm dia. retro-reflective targets spaced 25.4 mm apart. The scale tape manufacturer claims target spacing accuracy of +/- 0.025 mm. Because of the manufacturing accuracy of the scale tape it served not only as a tool in setting image scale but was also useful in evaluating the accuracy of the photogrammetry data.

Experimental Results

Ten data sets were collected, four using the cylinder with the 0.02 mm wall thickness and six with the 0.038mm wall thickness, with inflation pressures ranging from 137.9 Pa to 1379 Pa. Typical data for the targets located in the 12 x 5 grid are shown in Fig. 3. To determine the radius of the cylinder, regression was used to find the best-fit circle for the data points from each column of the grid. Due to variations in the seaming of the cylinder, the radius varied along the length of the cylinder. For the 0.02 mm wall thickness (0.8 mil), the radius varied as much as 1 mm at the higher pressures. Cylinders manufactured from the 0.038 mm (1.5 mil) thick material showed a variation in radius of approximately 0.3 mm. Table 1 gives the maximum, minimum and average radius for both cylinders for each test case. A single value for the cylinder radius was determined by averaging the data from the twelve sections. Figure 4a and 4b show the relationship between pressure and average radius for the two cylinders. Although there was variation in the radius of the cylinder along the length, the graphs show excellent correlation between the average radius and pressure.

Table 1. Variation in inflated cylinder radius.

	0.02 mm wall thickness				0.038 mm wall thickness					
Pressure (Pa)	344.7	448.2	999.7	1379	137.9	206.8	448.2	654.0	1069	1379
Max. radius (mm)	112.7	113.4	115.6	117.1	112.8	112.8	113.2	113.6	114.1	114.8
Min. radius (mm)	110.1	110.7	113.4	115.8	111.8	112.2	112.5	113.1	113.7	114.4
Average radius (mm)	111.3	112.0	114.5	116.3	112.3	112.4	112.8	113.3	113.9	114.6

Accuracy of Photogrammetry System

To evaluate the effectiveness of using photogrammetry to measure strain in balloon structures, the accuracy of the technique must be understood. To determine the accuracy of the technique we will consider the marking residual and the measured distance between targets of known spacing. The marking residual is the difference between where a mark was found on an image and where the photogrammetry software analytically determines the point should be. By looking at the largest marking residual error for each point, we can determine the quality of the data. The images used for this study covered approximately 740 x 520 mm of the balloon and frame. The 5.0 megapixel cameras used capture an image of 2560 x 1920 pixels. Therefore, the spatial resolution of the image was approximately 0.3 mm/pixel. The photogrammetry software uses a least squares method to determine the center of the circular targets in each image, which allows the center of the targets to be found to an accuracy of less than one pixel. An excellent description of the steps used to process multiple images are described in reference [15]. Table 2 provides data on the maximum, minimum, and average marking residual for each test case. Figure 5 is a histogram that shows the distribution for the marking residuals for all points located on the cylinder surface that were used for the test cases. The data in Table 2 and Fig. 6 indicate that the marking residuals were consistent across all the data sets. In all cases the average marking residual is less than 0.25 pixel and the largest marking residual of 0.46 pixels was seen for the 0.038 mm thick cylinder at a pressure of 137.9 Pa. The histogram shows that the distribution of the marking residuals is described by a normal distribution, which indicates that the marking errors are random.

Table 2. Data for marking residual for targets on cylinder surface for inflated cases.

Cylinder Wall Thickness	0.02 mm				0.038 mm					
Pressure (pa)	344.7	448.2	999.7	1379	137.9	206.8	448.2	654.0	1069	1379
Maximum marking residual (pixel)	0.3788	0.3412	0.3363	0.3637	0.4573	0.4315	0.4623	0.4173	0.4302	0.4412
Minimum marking residual (pixel)	0.0264	0.0454	0.0066	0.0144	0.0313	0.0308	0.0495	0.0451	0.0379	0.0592
Average marking residual (pixel)	0.1632	0.1554	0.1557	0.1649	0.2119	0.1620	0.1655	0.1583	0.1633	0.1918
Two St. Dev (95% Confidence)	0.1435	0.1276	0.1313	0.1450	0.1958	0.1473	0.1633	0.1368	0.1356	0.1841

To evaluate how the marking residual affected the determination of the three-dimensional coordinates, we evaluated the points along the scale tape for the data set with the largest marking residual (0.038 mm thick balloon at a Pressure of 137.9 Pa). As discussed previously, the scale tape used has 3 mm diameter retro-reflective targets spaced every 25.4000 +/- 0.0254 mm. Table 3 provides data on the maximum, minimum and average marking residual for the 23 targets on the scale tape and. Fig. 6 shows the corresponding histogram for the marking errors. Again the distribution of the marking residual indicates that the marking errors are random. Because the largest marking residual and average marking residual were both larger than those found for targets on the cylinder surface, this data is ideal for evaluating the accuracy of the measurements.

Table 3. Data for marking residual for fixed targets for 0.038 mm thick cylinder, P=137.9 Pa case.

Maximum marking residual (pixel)	0.8097
Minimum marking residual (pixel)	0.0707
Average marking residual (pixel)	0.2646
Two St. Dev (95% Confidence)	0.3022

Table 4 gives the measured x, y, and z coordinates of the centers of the 23 targets as well as the x, y, and z, spacing between targets. The last column in the Table gives the distance between target centers calculated using,

$$d = \sqrt{(x - x_0)^2 + (y - y_0)^2 + (z - z_0)^2} \quad . \tag{7}$$

Because the scale tape was chosen as the x axis for orienting the images and camera positions, the y and z coordinates should be very close to zero. This is indeed the case and thus the values calculated using Eqn (7) are similar to the values for the spacing of the targets in the x direction. The value of 25.3770 mm for the spacing in the x direction is within the expected range given the manufacturing tolerance of the scale tape. The measurement accuracy within a 95% confidence is less than 0.08 mm. Over the 740 mm of the cylinder surface captured in the image (targeted area plus additional non-targeted area) this corresponds to an accuracy of 1 part in 10,000 (1:10,000). The uncertainty of the measurement in the x direction of 0.079 mm indicates that using a gage length of 25.4 mm to determine strain may be insufficient to determine meridonal strain. The resulting uncertainty of 0.003110 mm/mm may be unacceptable.

Table 4. Spacing between adjacent fixed targets.

	x-coord. (mm)	y-coord. (mm)	z-coord (mm)	x spacing (mm)	y spacing (mm)	z spacing (mm)	d (mm)
	-279.123	-0.00758	0.234586				
	-253.794	-0.01132	0.152812	25.32885	-0.00374	-0.08177	25.32898
	-228.446	-0.0439	0.179059	25.34772	-0.03258	0.026247	25.34775
	-203.016	-0.04649	0.158133	25.43035	-0.00259	-0.02093	25.43036
	-177.666	-0.07425	0.100752	25.34955	-0.02776	-0.05738	25.34963
	-152.297	-0.07082	0.085768	25.36966	0.003429	-0.01498	25.36966
	-126.966	-0.05064	0.088395	25.33041	0.020184	0.002627	25.33041
	-101.535	-0.03929	0.054213	25.43161	0.011349	-0.03418	25.43164
	-76.178	-0.0035	0.045788	25.35662	0.035783	-0.00842	25.35664
	-50.8176	0.012692	0.048272	25.36036	0.016195	0.002484	25.36037
	-25.4229	0.004529	0.037906	25.39465	-0.00816	-0.01037	25.39465
	0	0	0	25.42295	-0.00453	-0.03791	25.42298
	25.38643	0.010383	0.011575	25.38643	0.010383	0.011575	25.38643
	50.71049	-0.01159	0.008874	25.32406	-0.02197	-0.0027	25.32407
	76.13362	-0.04169	-0.03024	25.42313	-0.0301	-0.03912	25.42318
	101.5733	-0.08187	-0.02319	25.4397	-0.04019	0.00705	25.43973
	126.9694	-0.10374	0.008654	25.39608	-0.02187	0.031848	25.39611
	152.2978	-0.13332	-0.00744	25.32836	-0.02957	-0.0161	25.32838
	177.7173	-0.18773	0.001159	25.41955	-0.05442	0.008601	25.41961
	203.1269	-0.21776	0.006099	25.40957	-0.03003	0.00494	25.40959
	228.4839	-0.21886	0.006119	25.35699	-0.0011	2E-05	25.35699
	253.8202	-0.21942	0.034745	25.33634	-0.00056	0.028626	25.33635
	279.1703	-0.17883	0.085867	25.35011	0.040589	0.051122	25.3502
Average				25.37696	-0.00778	-0.00676	25.37699
2 St. Dev (95% confidence)				0.078592	0.049132	0.061176	0.078583

The hoop and meridonal strains can be calculated based on a change in radius. In terms of minimizing uncertainty, this is the preferable method for determining the strain. The unstrained cylinder radius is approximately

111 mm. From Table 4 the accuracy of the measurements in the z direction were 0.061 mm. This gives an uncertainty in determining the change in radius of 0.000550 mm/mm.

IV. Analysis

Numerical Model

A mathematical model that has been used for the analysis of large scientific balloons was adapted to the cylinder problem and used to predict the hoop and length-wise strains. Because of the high-resolution and non-intrusive nature of photogrammetry, the cylinder inflation test provides an excellent benchmark for evaluating a mathematical model for a thin membrane structure. Although the cylinder is a relatively simple geometry, having a good correlation between predicted and measured strains in a well-controlled setting will give confidence when the same model is applied to more complicated scenarios (e.g. spool shapes) which cannot be reproduced in a laboratory setting at the appropriate scale. The details of the mathematical model presented here are given in refs. [19] & [20].

Large compliant structures such as high altitude scientific balloons are characterized by large deformations, but relatively small strains, typically on the order of one-percent. In the balloon model, a finite element method with piecewise linear elements is used to discretize the continuum problem of a pressurized envelope. The surface of the membrane is triangulated; an isotropic film is assumed and the elastic deformation is modeled assuming a linear constitutive relation and constant strain triangles (see ref. [19] for details). The equilibrium configuration of the pressurized membrane is the one that minimizes the potential energy of the system.

While it would be difficult to model the precise behavior of the membrane in the vicinity of the end-caps, for the purpose of the benchmark tests we are interested in the behavior of the membrane away from the end-caps. For this reason, we solve a proxy problem. We assume the membrane consists of three parts: a cylinder of diameter approximately 222 mm and length 914 mm and two disks that cap the ends of the cylinder. For simplicity, we assume the end-caps and cylinder are made of the same material. A typical configuration of the membrane in the proxy problem will be denoted by S. It's initial state is denoted by S^0 where,

$$S^0 = D_1^0 \cup C^0 \cup D_2^0 \tag{8}$$

$$\begin{aligned} C^0 &= \{(x,y,z) \mid (y-y_0)^2 + (z-z_0)^2 = r^2, x_1 < x < x_2\}, \\ D_1^0 &= \{(x,y,z) \mid (y-y_0)^2 + (z-z_0)^2 = r^2, x = x_1\}, \\ D_2^0 &= \{(x,y,z) \mid (y-y_0)^2 + (z-z_0)^2 = r^2, x = x_2\} \end{aligned} \tag{9}$$

In cylindrical coordinates, we let $y - y_0 = r\cos\theta$ and $z - z_0 = r\sin\theta$ for $-\pi < \theta < \pi$.

While the model in Ref. 19 includes straining of load tendons and contributions due to film and tendon weight, in our proxy problem there are no tendons and we ignore weight. The total energy of S is

$$E_T(S) = E_P(S) + S_{film}^*(S), \tag{10}$$

where E_P is the potential energy due to a constant pressure $P = p_0$, *i.e.,*

$$E_P(S) = -\int_S \frac{1}{2} p_0 y \mathbf{j} \cdot \mathbf{n} dS, \tag{11}$$

n is the outward unit normal to S; S_{film} is the strain energy of the film, i.e.,

$$S_{film}(S) = \int_{\Omega} W_f^* dA, \tag{12}$$

where W_f^* is the relaxed film strain energy density and _ is the corresponding reference configuration. Away from the end caps there is little wrinkling, and for a triangle T that is in a taut state, the relaxed strain energy density is the same as the standard membrane strain energy density (i.e., $W^*_f(S) = W_f(S)$) and

$$W_f^*(T) = \frac{tE}{2(1-\nu^2)}\left(\varepsilon_1^2 + \varepsilon_2^2 + 2\nu\varepsilon_1\varepsilon_2\right), \tag{13}$$

where ε_1 and ε_2 are the principal strains. The principal strains are related to the principal stress resultants by,

$$\begin{Bmatrix}\varepsilon_1\\ \varepsilon_2\end{Bmatrix} = \frac{Et}{1-\nu^2}\begin{Bmatrix}\sigma_1 + \nu\sigma_2\\ \sigma_2 + \nu\sigma_1\end{Bmatrix}. \tag{14}$$

To compute an equilibrium configuration of a pressurized cylinder, we solve the following variational problem:

$$\min_{s\in u} E_T(S) \tag{15}$$

where u is the set of all feasible configurations satisfying the boundary conditions.

We computed solutions for one-half of a cylinder, $-\frac{1}{2}\pi < \theta < \frac{1}{2}\pi$, and for one-tenth of a cylinder, $-\frac{1}{20}\pi < \theta < \frac{1}{20}\pi$, and found there was little difference in the averaged hoop and meridional strains. So for the calculations that we presented here, we consider a slice of *S* that is only one-tenth of the circumference of the cylinder.

In our model we compute the principal strains for each facet in our discretization of *S*. Ignoring those triangles that make up the end-caps, we compute the average of the principle strains, ε_1, hoop strain, and ε_2, meridian strain. The average of the ε_1's is denoted by ε_H^P. The average of the ε_2's is denoted by ε_M^P.

Estimating Membrane Strains from Photogrammetry Data

The length-wise (meridonal) strains were computed directly from the data by determining the change in spacing between adjacent targets as the cylinder is inflated. Let $\left(x_{ij}^0, y_{ij}^0, z_{ij}^0\right)$ for i=1, 2,, . . . , 12, and j=1,….,5.

Let $L_{ij} = x^0_{i+1,j} - x^0_{ij}$, If $\left(x_{ij}^k, y_{ij}^k, z_{ij}^k\right)$ are the location of the targets for Pressure Epoch k, then the length-wise strains are given by

$$\frac{x_{i+1,j}^k - x_{i,j}^k}{L_{i,j}}, i = 1,2,.....,11, j = 1,2,....5. \tag{16}$$

These values are then averaged to yield a single length-wise strain, ε_M.

The hoop strains are estimated by determining the change in radius of the cylinder during inflation. For Epoch k, we find the best circle, in the least square's sense, that fits each of the bands, i=1,…., n_M. We find $\left(\hat{y}_{c,i}, \hat{z}_{c,i}\right)$ and $\hat{r}_i$ that minimizes the sum of the squares of the residuals, i.e.,

$$\min_{(y_c, z_c, r)} \sum_{j=1}^{5} \left| \left(y_{ij} - y_c\right)^2 + \left(z_{ij} - z_c\right)^2 - r^2 \right|^2 . \tag{17}$$

The radii, $\hat{r}_i$, are averaged to yield a single radius, $\bar{r}^{(k)}$, for the entire cylinder for Epoch k. If r_o is the radius calculated in this fashion for the initial state k=0, the hoop strain is given by

$$\varepsilon_H = \frac{2\pi\bar{r}^{(k)} - 2\pi r_o}{2\pi r_0} = \frac{\bar{r}^{(k)} - r_o}{r_0} . \tag{18}$$

In practice, the radius at a zero pressure is difficult to obtain so we found it best to use one of the early epochs to define r_o.

The material properties were not measured and there is considerable variation in the properties in the published literature. To evaluate the numerical algorithm the material properties were determined from the experimental data as described above. For the geometry defined by the experiment, using Eqns (3) and (4), the hoop stress is twice the meridonal stress. This gives a simple way of corroborating the predictions in the model. Once we estimate the hoop strains using the photogrammetry data, these values can be substituted into Eqn (14), because $(\square_1,\square_2)=(\square_\square,\square_\square)$, and solve the resulting system for E and $\square$ for each Epoch k using the analytical solution. The primary focus of this study is to evaluate the measurement system.

Comparison of Experimental and Theoretical Results

For each Epoch we solved the problem described in Eqn (5) and determined the principal strains for each facet within the target grid. In Fig. 7, the strains determined from the experimental data are plotted for the cylinder with the 0.020 mm wall thickness at P_0=999.7. Similar plots were obtained for other pressure Epochs. For this case using Eqns (3) and (4) we determine that the hoop stress resultant should be 114.27 N/m and the meridonal stress resultant should be 57.13 N/m. From the numerical results, we determined that the average hoop and meridonal stress resultants were 113 N/m and 59 N/m, respectively. In Table 5, for the 0.02 mm wall thickness cylinder we compare the average principal strains that were determined from the experimental data with the strains predicted by the model. Table 6 compares similar data for the cylinder manufactured from 0.038mm thick material. As discussed previously, the material properties were estimated using the experimental data and Eqn (14). This allowed us to evaluate the performance of the algorithm without accounting for the uncertainty or anisotropy in the material properties. Using this approach the maximum relative error in the hoop strains is 3.6%. The length-wise (meridonal) strain results for the lowest pressure epochs were comparable. However, the relative error jumps dramatically for the two highest pressure epochs.

Table 5. Comparison of measured and predicted strains for cylinder with 0.020 mm wall thickness.

	Measured						Predicted					
Epoch	Pressure (Pa)	$r^{(k)}$ (mm)	$\square_H$	$\square_M$	$E(P_0)$ (Mpa)	$\square(P_o)$	$\square_H^P$	$\square_M^P$	$\left\|\frac{\square_H-\square_H^P}{\square_H}\right\|$	$\left\|\frac{\square_M-\square_M^P}{\square_M}\right\|$	$\square_H$ (N/m)	$\left\|\frac{P_o r^{(k)}-\square_H^P}{P_o r^{(k)}}\right\|$
0	27.6	113.18	N/A	N/A	N/A	N/A	0.00030	-0.00009	N/A	N/A	N/A	N/A
1	344.7	113.60	0.00376	-0.00111	334.4	0.69	0.00376	-0.00110	0.0011	0.0126	39.3	0.0047
2	448.2	113.77	0.00521	-0.00164	311.5	0.70	0.00520	-0.00160	0.0031	0.0255	51.2	0.0033
3	999.7	114.78	0.01419	-0.00269	272.4	0.63	0.01390	-0.00236	0.0207	0.1238	114.0	0.0067
4	1379	115.81	0.02322	-0.00320	237.4	0.60	0.02239	-0.00237	0.0359	0.2585	157.1	0.0159

Table 6. Comparison of measured and predicted strains for cylinder with 0.038mm wall thickness.

	Measured						Predicted					
Epoch	Pressure (Pa)	$r^{(k)}$ (mm)	$\square_H$	$\square_M$	$E(P_0)$ (Mpa)	$\square(P_o)$	$\square_H^P$	$\square_M^P$	$\left\|\frac{\square_H-\square_H^P}{\square_H}\right\|$	$\left\|\frac{\square_M-\square_M^P}{\square_M}\right\|$	$\square_H$ (N/m)	$\left\|\frac{P_o r^{(k)}-\square_H^P}{P_o r^{(k)}}\right\|$
0	27.58	112.64	N/A	N/A	N/A	N/A	0.00011	-0.00005	N/A	N/A	N/A	N/A
1	448.2	112.80	0.00146	-0.00132	466.7	0.97	0.00146	-0.00132	0.0006	0.0007	51.1	0.0099
2	655.0	113.25	0.00548	-0.00173	229.8	0.70	0.00549	-0.00170	0.0018	0.0196	74.8	0.0079
3	1069	113.90	0.01125	-0.00215	194.2	0.63	0.01114	0.00195	0.0100	0.0924	121.9	0.0012
4	1379	114.56	0.01711	-0.00300	167.0	0.62	0.01675	-0.00254	0.0214	0.1541	157.1	0.0052

To better understand the uncertainty in the measurement and it's effect on strain we recalculated the strain using

$$\frac{x_{i+3,j}^k \square x_{i,j}^k}{L_{i+3,j}}, i = 3,6,9\ j = 1,2,....,5 \tag{19}$$

rather than Eqn (16). Using Eqn (19) increased the gauge length by three times. Dividing the measurement uncertainty by the gauge length gave and uncertainty in the merdional strain of 0.000919. Increasing the gauge

length lowers the uncertainty in the meridional strain measurement by an order of magnitude. Table 7 compares strain calculations based on Eqn (16) and those based on Eqn (19) for the cylinder with 0.02 mm wall thickness.

Table 7. Comparison between strains calculated using gauge lengths of 25.4 and 76.2mm.

Epoch	L=25.4	L=76.2	ε_M
1	-0.001115	-0.001118	0.000003
2	-0.001647	-0.001636	0.000011
3	-0.002700	-0.002662	0.000038
4	-0.003207	-0.003195	0.000012

V. Discussion

Measuring strain in scientific balloons or other structures that employ thin films is a difficult task dictating the use of non-contact measurement techniques. Currently, the two leading technologies, both based on digital imaging, are random speckle techniques and photogrammetry using circular targets. In ref [13] the authors demonstrate the use of a single CCD imager and measure the relative displacement of speckles on an inflated cylinder. It is also possible to use multiple imagers rather than a single imager. Speckle techniques using multiple imagers can be thought of as very close range photogrammetry. Speckle techniques provide strain measurements over a small area, while photogrammetry is suitable for assessing the global or average strain. For a relatively simple geometry like the cylinder, the two methods should yield similar results, although the uncertainty in the measurement will be lower for the speckle technique as the targeted area, although small, will fill the camera field of view. The drawback to the speckle technique is that it requires the membrane to be coated with a layer of white paint or talc followed by a "speckling" or thin layer of black paint. These coatings are easily damaged and are not suited for folding and inflation type testing, or for use on a flight experiment. If photogrammetry is to be used to measure strain, targets must also be attached to the balloon surface. The retro-reflective targets used for this study were 3mm in diameter and weighed approximately 0.004 g each. The 60 targets used for the study added less than 0.25 g to the mass of the cylinder. Fixed retro-reflective targets can be used for folding and inflation testing and are suitable for use during a flight experiment.

Because the accuracy of photogrammetry data depends on intersecting rays of light, the measurement uncertainty is project specific. The accuracy of photogrammetry data is dependent on the number of cameras used, camera locations and spacing, camera resolution, lens calibration, lighting, type of target, and proper scaling of the image. The data shown in Tables 5 and 6 indicate a reasonable agreement between the analysis and the experiment. Table 7 indicates that although the gauge length is tripled the strain value remains unchanged. The accuracy was determined from adjacent targets on a scale tape whose target spacing was 25.4 +/- 0.0254 mm. The measured value was 25.377 +/- 0.08mm, but the actual measurement uncertainty is likely less than 0.08mm because 25.377 lies within the manufacturing uncertainty. Although an overall accuracy of 1:10,000 is excellent this value doesn't provide insight into how accurately the data measures relative motions of targets. This project demonstrates the need for targets of known spacing to be distributed throughout the image.

VI. Conclusion

A study of biaxial strain in an inflated cylinder has been presented. Photogrammetry using fixed retro-reflective targets was used as the measurement technique. The data showed a reasonable agreement with the numerical analysis. The hoop strains agreed with the experimental data within 3.6% while the meridonals strains agreed with the analysis at the lower pressure epochs. Overall the accuracy of the photogrammetry system was 1:10,000. This produced and uncertainty of 0.08 mm for measurements along the length of the cylinder (x direction) and 0.06 mm in the z direction.

References

References

Note: Items available in the NASA Balloon Technology Library are denoted by their identifier in that system, such as BT-1037. Contact beddy@pop200.gsfc.nasa.gov for access information.

1. Stautgaitis, C.L., and L. Kobren, "Strain Measurements Conducted on a Full Scale Echo II Passive Communications Satellite Balloon," NASA TN D-3126, Accession No. N66-19752, July 1965.
2. Simpson, J.M., "Model Balloon Strain Field Survey – Test Results," NASA Scientific Balloon Program Report, October 1987 (BT-1668).
3. Simpson, J.M., "Comparison of ABAQUS Analysis and Measured Strains for 17,000 ft^3 Scientific Balloon," NASA Scientific Balloon Program Report, October 1989 (BT-1673).
4. Martone, M., "Long Duration Biaxial Cylinder Testing of Balloon Grade Polyethylene Films with Emphasis on Automated Data Acquisition and Control," *Adv. Space Res.*, v.14, n.2, pp. 21-25, 1994 (BT-2475.03).
5. Said, M.A., "A Novel Technique for Measuring Strains in Thin Films Under Biaxial Conditions," *ANTEC 94 Proceedings*, Society of Plastics Engineers, vols. 1-3, pp. 2272-2275, 1994.
6. Said, M.A., "Biaxial Test Method for Characterization of Fabric-Film Laminates Used In Scientific Balloons," *ANTEC 2000 Proceedings*, Society of Plastics Engineers, vols. I-III, pp. 1593-1596, 2000.
7. Rand, J.L., and D.A. Grant (Fairbrother), "Optical Measurement of Biaxial Strain in Thin Film Polymers," in *Nontraditional Methods of Sensing Stress, Strain, and Damage in Materials and Structures, ASTM STP 1318*, edited by Lucas and Stubbs, American Society for Testing and Materials, Philadelphia, 1997.
8. Rand, J.L., D.A. Grant (Fairbrother), and T. Strganac, "The Nonlinear Biaxial Characterization of Balloon Film," AIAA Paper No. 96-0574, *34th Aerospace Sciences Meeting & Exhibit*, Reno, January 1996.
9. Pappa, R.S., Lassiter, J.O., and Ross, B.P., "Structural Dynamics Experimental Activities in Ultra-Lightweight and Inflatable Space Structures," *Journal of Spacecraft and Rockets*, Vol. 40, No. 1, Jan.-Feb. 2003, pp. 15-23.
10. Alexander, H., "Creep Characteristics of Polyethylene Film," *Proceedings of the 4th Air Force Cambridge Research Laboratories Scientific Balloon Symposium*, Ed. J.F. Dwyer, AFCRL-67-0075, January 1967 (BT-1037.03).
11. Kawada, K., et al., "The Measurement of Strain in Balloon Films," translated for the U.S. Air Force Cambridge Research Laboratories from *Tokyo University Institute of Space and Aeronautical Science Bulletin*, 3(2B):398-401, 1967 (BT-1476).
12. Kawada, K., et al., "Measurement of the Strength of Polyethylene Films and the Strain During Balloon Flight," translated for the U.S. Air Force Cambridge Research Laboratories from *Tokyo University Institute of Space and Aeronautical Science Bulletin*, 5(1B):106-116, 1969 (BT-1474).
13. Rand, J.L., "Thin Film Strain Transducer," U.S. Patent No. 4 498 231, Feb. 12, 1985 (BT-2270).
14. Rand, J.L., "Balloon Film Strain Measurement," *Adv. Space Res.*, v.3, n.6, pp. 45-48, 1983 (BT-2470.06).
15. Pappa, R.S., Geirsch, L.R., and Quagliaroli, J.M., "Photogrammetry of a 5-m Inflatable Space Antenna with Consumer-Grade Digital Cameras," *Experimental Techniques*, July/August 2001, pp. 21-29.
16. Jones T.W. and Pappa, R.S., "Dot Projection Photogrammetric Technique for Shape Measurements of Aerospace Test Articles," AIAA Paper 2001-1263, April 2001.
17. Blandino, J.R., Johnston, J.D., and Dharamsi, U.K., "Corner Wrinkling of a Square Kapton Membrane," *Journal of Spacecraft and Rockets*, Vol 39, No. 5, Sept-Oct 2002, pp. 717-724.
18. Blandino, J.R., Johnston, J.D., Miles, J.J., and Dharamsi, U.K., "The Effect of Asymmetric Mechanical and Thermal Loading on Membrane Wrinkling," AIAA Paper 2002-1371, *Proceedings of the 43rd AIAA Structures, Structural Dynamics and Materials Conference*, Denver, CO, 22-25 April, 2002.
19. Baginski, F and Collier, W., "Modeling the Shapes of Constrained Partially Inflated High Altitude Balloons," *AIAA J.,* Vol 39, No. 9, Sept, 2001, pp. 1662-1672., Errata: *AIAA J*., Vol. 40, No. 9, Sept 2002.
20. Baginski, F., and Schur, W., "Structural Analysis of Pneumatic Envelopes: A Variational Formulation and Optimization Based Solution Process, *AIAA J*., Vol. 41, No. 2, 2003, 304-311.

Acknowledgement

The authors would like to thank Kiley C. McEvoy and John M. Petek, Undergraduate Research Assistants in the Department of Integrated Science and Technology at James Madison University, for their help in collecting photogrammetry data for this project. This work was supported in part by NASA Grant NAG5-5353.

(a)Front View (b)Side View

Figure 1. Test set-up.

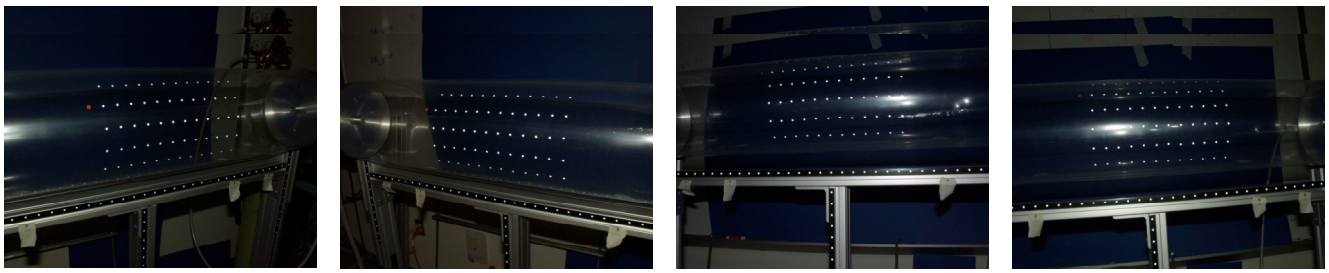

Figure 2. Photogrammetry image set.

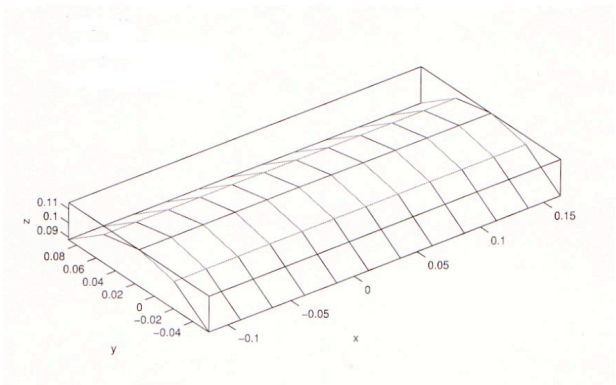

Figure 3. Typical data for targeted area of cylinder.

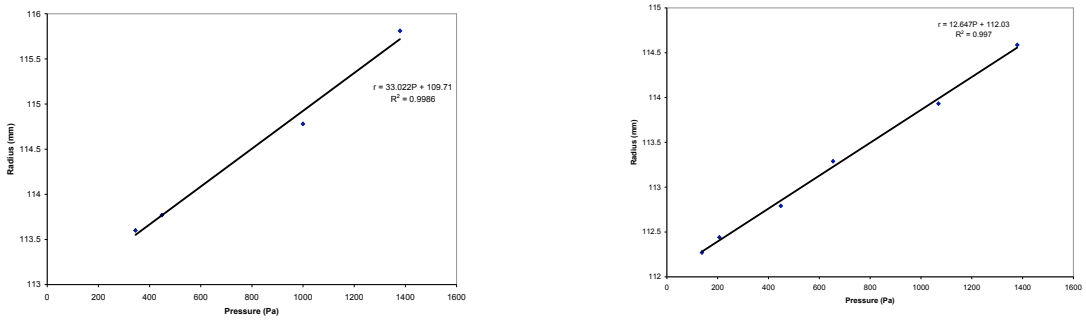

(a) 0.02 mm wall thickness (b) 0.038 mm wall thickness

Figure 4. Average cylinder radius as a function of pressure.

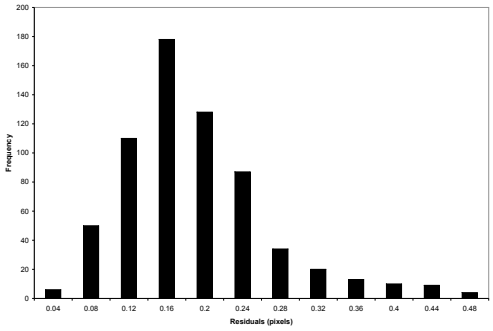

Figure 5. Histogram of marking residuals for all points on cylinder surface.

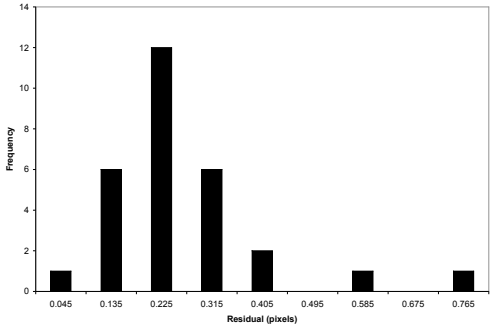

Figure 6. Histogram of marking residuals for fixed target on test frame.

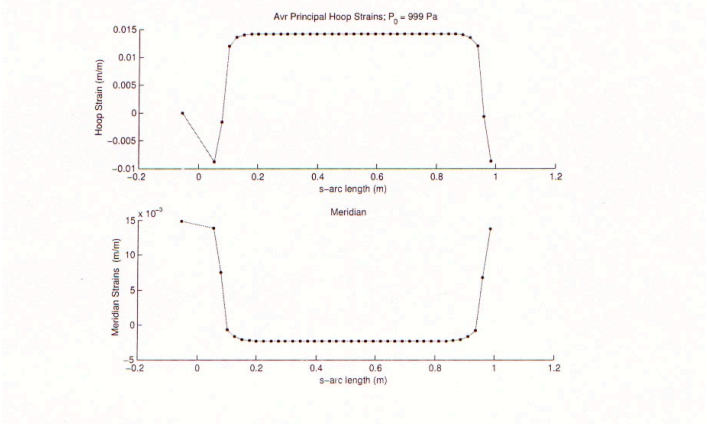

Figure 7. Predicted strains from FEA of cylinder proxy problem with 0.02 mm wall thickness.